REPORT DOCUMENTATION PAGE

Form Approved
OMB No. 0704-0188

PLEASE DO NOT RETURN YOUR FORM TO THE ABOVE ORGANIZATION.

1. REPORT DATE *(DD-MM-YYYY)*	2. REPORT TYPE	3. DATES COVERED *(From - To)*
08-10-2012		09/16/2009 - 09/15/2012

4. TITLE AND SUBTITLE

Shock Response and Dynamic Failure of Spatially Tailored Aero-Thermal Structures

5a. CONTRACT NUMBER

5b. GRANT NUMBER

FA9550-09-1-0639

5c. PROGRAM ELEMENT NUMBER

6. AUTHOR(S)

Arun Shukla

5d. PROJECT NUMBER

5e. TASK NUMBER

5f. WORK UNIT NUMBER

7. PERFORMING ORGANIZATION NAME(S) AND ADDRESS(ES)

University of Rhode Island
92 Upper College Road, Kingston, RI, 02881

8. PERFORMING ORGANIZATION REPORT NUMBER

9. SPONSORING/MONITORING AGENCY NAME(S) AND ADDRESS(ES)

AFOSR
875 N Randolph St
Arlington, VA 22203
Dr. David Stargel/RSA

10. SPONSOR/MONITOR'S ACRONYM(S)

11. SPONSOR/MONITOR'S REPORT NUMBER(S)

AFRL-OSR-VA-TR-2012-1236

12. DISTRIBUTION/AVAILABILITY STATEMENT

Distribution A-Approved for Public Release

13. SUPPLEMENTARY NOTES

14. ABSTRACT

A comprehensive study was conducted to evaluate the performance of spatially tailored aero-thermal structures under thermo-mechanical loadings. Starting from the first principles, analytical analyses were conducted to develop thermo-mechanical stress fields for mixed mode dynamic curving cracks in functionally graded materials (FGMs) under steady-state and transient loading conditions. Asymptotic analysis was used in conjunction with displacement potentials to develop the stress fields around propagating cracks in FGMs. The effect of crack path curvature, transient parameters, temperature and gradation on various components of stresses were evaluated and discussed. Experimental studies were then conducted to evaluate two different materials, namely, Hastelloy X and Nanolayered Titanium Aluminum Carbide (a MAX phase material) under varying rates of loading and at different temperatures. The Johnson-Cook parameters were determined for Hastelloy X to predict its dynamic plastic response at different temperatures and strain rates. A unique high temperature set up was also developed to study these materials at extreme tem

15. SUBJECT TERMS

Functionally Graded Materials, Dynamic Constitutive Behavior, Hastelloy X, Thermo-mechanical Stress Fields, Curved Crack

16. SECURITY CLASSIFICATION OF:			17. LIMITATION OF ABSTRACT	18. NUMBER OF PAGES	19a. NAME OF RESPONSIBLE PERSON
a. REPORT	b. ABSTRACT	c. THIS PAGE			Dr. Arun Shukla
U	U	U	U	17	19b. TELEPHONE NUMBER *(Include area code)* 401-874-2283

Reset

Standard Form 298 (Rev. 8/98)
Prescribed by ANSI Std. Z39.18

Dr. David S. Stargel
Program Manager
Aerospace, Chemical and Materials Science Directorate
DEPARTMENT OF THE AIR FORCE
Air Force Office of Scientific Research (AFRL)
875 North Randolph Street
Arlington VA 22203-1977

FINAL PERFORMANCE REPORT

Shock Response and Dynamic Failure of Spatially Tailored Aero-Thermal Structures

ARUN SHUKLA
Simon Ostrach Professor
Dynamic Photomechanics Laboratory
Department of Mechanical, Industrial and Systems Engineering
University of Rhode Island
Kingston, RI 02881
USA

ACCOMPLISHMENTS

A project entitled "Shock Response and Dynamic Failure of Spatially Tailored Aero-Thermal Structures" was funded by the AFOSR for a period of 3 years (September 2009 to September 2012). During this project, several accomplishments were made and these include: (a) Dynamic constitutive behavior of Hastelloy X at extreme temperatures under high strain rates of loading. (b) Analytical analyses to develop the thermo-mechanical stress and strain fields for mixed-mode dynamic crack growth along an arbitrary, smoothly-varying, curved path in FGMs under steady-state and transient loading conditions. (c) High strain rate behavior of Nanolaminated Titanium Aluminum Carbide (a MAX phase material) and ZrB_2 materials. (d) Development of unique facility for testing materials at high temperature under shock loading. To date, this work has produced (6) journal papers and (4) proceedings papers. Also, (1) additional journal paper has been submitted for publication. The following objectives have been successfully achieved during this project.

Objectives

- *Dynamic constitutive behavior of Hastelloy X under thermo-mechanical loads.*
- *Development of Johnson-Cook constitutive model for Hastelloy X at different temperatures and strain rates.*
- *Analytical development of steady-state and transient stress, strain and displacement fields for propagating curved cracks in FGMs subjected to combined and rapidly changing thermo-mechanical loading.*
- *An overview of optical investigations was reviewed for both quasi-static and dynamic fracture investigations involving mode-I and -II conditions.*
- *High strain rate behavior of Ti_2AlC at extreme temperatures.*
- *High strain rate behavior of ZrB_2 at room temperature.*
- *Development of unique set up for testing materials at high temperatures (up to 1000°C) under shock loading.*

SUMMARY

The objective of this study was to help in the development of spatially tailored aero-thermal-structures **(STATS)** that eliminate high-maintenance, parasitic, external thermal protection systems and integrate the thermal-load carrying function within the structure. For this purpose, analytical thermo-mechanical stress fields were developed for propagating curved cracks in FGMs under steady-state and transient loading conditions. A comprehensive series of experiments were conducted to study the dynamic response of Hastelloy X and Ti_2AlC under thermo-mechanical loads. A unique high temperature/extreme environment experimental test facility was built for testing materials under shock loading up to 1000°C. The specific deliverables of the project are summarized as follows:

1. Dynamic Constitutive Behavior of Hastelloy X under Thermo-Mechanical Loads

An experimental investigation was conducted to study the dynamic constitutive behavior of Hastelloy X (AMS 5754) at room and elevated temperatures under varying rates of loading. A Split Hopkinson Pressure Bar (SHPB) apparatus was used in conjunction with an induction coil heating system for applying dynamic loads at elevated temperatures. Experiments were carried out at different temperatures ranging from 25°C to 1100°C at an average strain rate of $5000s^{-1}$. Room temperature experiments were performed out at varying strain rates from $1000s^{-1}$ to $4000s^{-1}$. The results show that as the strain rate was increased from quasi-static to $4000s^{-1}$, the value of yield strength increased by approximately 50%. Also, under dynamic loading, the yield stress decreased with temperature up to 700°C, after which it showed a peak at 900°C before beginning to decrease again as the temperature was further increased. The Johnson-Cook model was used to predict the dynamic plastic response under varying rates of loading and at different temperatures. This work has been published and more details can be found in the published article [Section 9, Ref 4].

2. Dynamic Curving Cracks in Functionally Graded Materials under Thermo-Mechanical Loading

Mixed-mode dynamic crack growth along an arbitrary smoothly varying path in FGMs was studied under thermo-mechanical loading conditions. The property gradation in FGMs was considered by varying shear-modulus, mass density, thermal conductivity and coefficient of thermal expansion exponentially along the gradation direction. Asymptotic analysis in conjunction with displacement potentials was used to develop the stress fields around propagating cracks in FGMs. Asymptotic temperature fields were first developed for the exponential variation of thermal conductivity and later these temperature fields were used to derive thermo-mechanical stress fields for a curving crack in FGMs. Using these thermo-mechanical stress fields, various components of the stresses were developed and the effect of curvature parameters, temperature and gradation on these stresses were discussed. Finally, using the minimum strain energy density criterion, the effect of curvature parameters, crack-tip speeds, non-homogeneity values and temperature gradients on crack growth directions were determined and discussed. This work has been published and more details can be found in the published article [Section 9, Ref 5].

3. Transient Thermo-mechanical Analysis of Dynamic Curving Cracks in Functionally Graded Materials

Asymptotic analysis in conjunction with displacement potentials was used to develop transient thermo-mechanical stress fields for mixed mode dynamic curving cracks in FGMs. Asymptotic temperature field equations were derived for exponentially varying thermal properties, and later these equations were used to derive transient thermo-mechanical stress fields for a curving crack in FGMs. The effect of transient parameters (loading rate, crack-tip acceleration, and temperature change) and temperature gradient on the maximum principal stress and circumferential stress associated with the propagating crack-tip was discussed. Finally, using the minimum strain energy density criterion, the effect of temperature gradient, crack-tip speeds and T-stress on crack

growth directions were determined and discussed. This work has been published and more details can be found in the published article [Section 9, Ref 6].

4. Experimental Fracture Mechanics of Functionally Graded Materials: An Overview of Optical Investigations

The experimental efforts towards understanding the fracture behavior of continuously graded FGMs using full-field optical methods were reviewed. Both quasi-static and dynamic fracture investigations involving mode-I and -II conditions were presented. FGM configurations with crack planes perpendicular to, parallel to and inclined to the direction of compositional gradation were discussed. Different strategies adopted by various investigators to develop polymer-based FGM systems for experimental mechanics studies were also described in this overview. Major theoretical developments that have predated and paralleled the experimental studies were presented as well. Finally, a few potential new directions where further contributions are possible were listed. This work has been published and more details can be found in the published article [Section 9, Ref 3].

5. Effect of Strain-rate and Temperature on Dynamic Deformation of Nanolaminated Ti2AlC

Nanolaminated ternary carbide, Ti_2AlC, was characterized under dynamic loading using a SHPB compression apparatus. The dynamic loading experiments were performed in the strain rate range of 1500-4200s^{-1} and at temperatures ranging from room temperature to 1150°C. At room temperature, the failure stress and strain showed little dependence on strain rate, whereas the failure stress drops considerably at temperatures above 900^{o}C. At all strain rates and temperatures, Ti_2AlC exhibited softening after failure initiation and a more graceful failure due to delamination and kink band (KB) formation. At temperatures higher than 900°C, grain boundary decohesion was suggested to contribute towards the decrease in the failure stress. The details of this study are attached in Appendix 1 and the manuscript has been submitted for publication.

6. Effect of Strain-rate and Temperature on Dynamic Deformation of Nanolaminated Ti2AlC

A series of experiments were conducted to study the dynamic compressive behavior of ZrB_2-SiC at different strain rates. Experiments were performed for three different strain rates ranging from 750-1600s^{-1} using a split Hopkinson pressure bar apparatus. The details of this work are attached in Appendix2.

7. Experimental Facilities Developed

During the later part of the grant, a unique facility for high temperature testing under shock loading was established. The salient features of this facility are discussed below.

7.1 High Temperature Experimental Setup

Various techniques were investigated to effectively achieve uniform heating of the specimens during the shock loading experiments. Initially, the use of an induction coil heating system was considered to heat the specimen to very high temperatures. Due to the restrictions of the loading apparatus, the coils could not be present at the center of the

specimen. This failed to provide a uniform temperature across the entire length of the specimen and thus another heating technique had to be considered. After visiting the Air Force facilities at Wright-Patterson Air Force Base, infrared heaters using quartz lamps was considered based on their ability to reach very high temperatures while offering ample control. The quartz lamps have to be placed very close to the specimen to direct most of the heat onto the specimen. Later, it was determined that quartz lamps would not be suitable to withstand the intense and violent loads developed during shock loading.

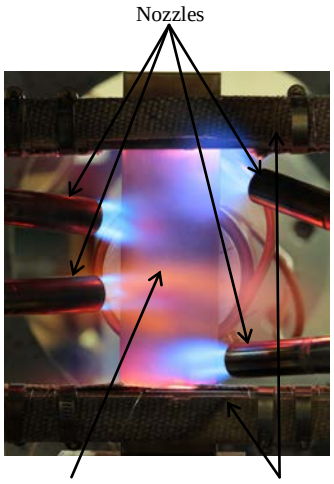

Fig. 1 Front-view of the modified shock tube setup

After discussing with Dr. Ken Leger, Dr. Tom Eason and Dr. Ravi Chona from the Air Force Research laboratory, it was decided to use propane gas as the heating source to effectively provide an extreme heating environment that is both robust and capable of providing uniform heating during shock loading. The propane gas is directed onto the specimen via four nozzles as shown in Fig. 1. Two nozzles were located on each side of the specimen and they were angled on different locations of the specimen. The nozzles on the left side were directed at the center of the specimen, while the nozzles on the right side were directed at the top and bottom of the specimen. Different temperatures are obtained by adjusting the distance between the specimen and the nozzles. For each temperature, the angle and the intensity of the flame of all the four nozzles were adjusted to obtain uniform heating of the specimen between the supports. The temperature on the specimen was monitored at three different locations between the supports using a chromel-alumel thermocouple to ensure uniform temperature distribution on the specimen. The temperatures recorded at these locations are shown in Fig. 2. It can be seen that a uniform temperature of about 900°C was achieved between the supports with a maximum gradient of $\pm$15°C. To protect the supports, a high temperature flame resistant paint was applied and then wrapped with a heat shield. A cooling system was also implemented to prevent the shock tube from reaching high temperatures. This was crucial in protecting the highly sensitive pressure sensors located towards the end of the muzzle. The cooling system shown in Fig. 3 consists of a copper coil tightly wound around the muzzle end in which tap water is circulated. Both systems together allow the specimen to be heated to temperatures exceeding 1000°C while protecting the surrounding equipment, thus allowing for precise

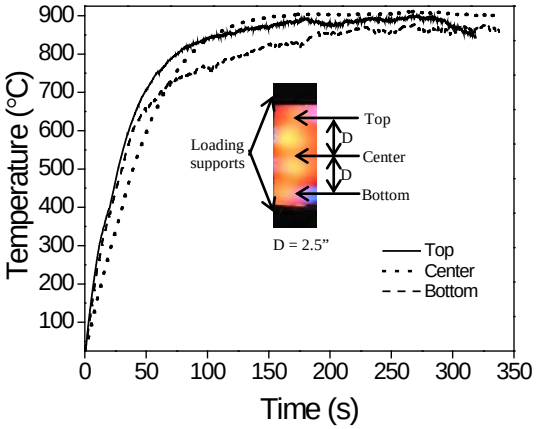

Fig. 2 Calibration curve for 900°C

pressure measurements during each test. The temperature at the center of the specimen is monitored simultaneously using an infrared thermometer.

To obtain the real-time strain and displacement fields, a 3D digital image correlation system will be utilized. Speckle patterns will be applied using high temperature flame proof paint. A side-view camera will also be used to obtain the deflections exhibited by the specimens at different temperatures under extreme shock loading. A series of trial experiments have been performed to validate the operation and performance of the experimental setup.

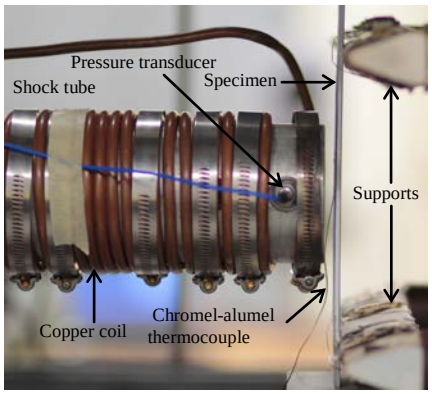

Fig. 3 Side-view of the modified shock tube setup with cooling set up

8. Student Supported: Sandeep Abotula (Ph.D).

9. Archival publications (published) during reporting period:

1. Kidane, A., Shukla, A. Quasi-static and Dynamic Fracture Initiation Toughness of Ti/TiB Layered Functionally Graded Material under Thermo-Mechanical Loading. *Engineering Fracture Mechanics*. **77** (3), 479-491, 2010.
2. Kidane, A., Chalivendra., Shukla, A., Chona. Mixed-mode Dynamic Crack Propagation in Graded Materials under Thermo-Mechanical Loading. *Engineering Fracture Mechanics*. **77** (14), 2864-2880, 2010.
3. Rousseau, C, E., Chalivendra, V, B., Tippur, H, V., Shukla, A. Experimental Fracture Mechanics of Functionally Graded Materials: An Overview of Optical Investigations. *Experimental Mechanics*. **50**, 845-865, 2010.
4. Abotula, S., Shukla, A., Chona, R. Dynamic Constitutive Behavior of Hastelloy X under Thermo-Mechanical Loading. *Journal of Material Science.* **46**, 4971-4979, 2011.
5. Abotula, S., Kidane, A., Chalivendra, V. B., Shukla, A. Dynamic Curving Cracks in Functionally Graded Materials under Thermo-Mechanical Loading. *International Journal of Solids and Structures.* **49** (13)**,** 1637-1655, 2012.
6. Gupta, S., Abotula, S., Chalivendra, V. B., Shukla, A., Chona R. Transient Thermo-Mechanical Analysis of Dynamic Curving Cracks in Functionally Graded Materials. *Acta Mechanica*. **223** (7), 1485-1506, 2012.

10. Archival publications (submitted) during reporting period:

1. Abotula, S., Basu, S., Radovic, M., Shukla, A. Effect of Strain-rate and Temperature on Dynamic Deformation of Nanolaminated Ti_2AlC. *Acta Materialia*. **Submitted**, 2011.

11. Conference, Proceedings Publications:

1. Kidane, A., Chalivendra, V. B., Shukla, A. Effect of Temperature and Crack Tip Velocity on the Crack Growth in Functionally Graded Materials. SEM 2010 Annual

Conference & Exposition on Experimental & Applied Mechanics, June 7-10, 2010, Indianapolis, Indiana.

2. Abotula, S., Shukla, A., Chona, R. Dynamic Constitutive Behavior and Fracture Initiation Toughness of Hastelloy X under Thermo-Mechanical Loads. Implast Conference. October 12-14, 2010, Providence, Rhode Island.
3. Abotula, S., Shukla, A., Chona, R. Dynamic Constitutive Behavior of Hastelloy X under Thermo-Mechanical Loads. SEM Annual Conference & Exposition on Experimental and Applied Mechanics Accepted for poster presentation, June 13 - 16, 2011, Mohegan Sun, Uncasville, Connecticut.
4. Abotula, S., Basu, S., Radovic, M., Shukla, A. High Strain Rate Deformation Behavior of Nanolaminated Titanium Aluminum Carbide. 36th International Conference and Exposition on Advanced Ceramics and Composites, January 22-27, 2012, Daytona Beach, Florida.

12. Invited Lectures

1. Seminar at University of Illinois Urbana-Champaign, 2010.
2. Seminar at Boston University, 2010.
3. Seminar at Texas A&M University, 2011.
4. Seminar at Caltech University, 2011.
5. Seminar at University of California, San Diego, 2011.
6. Seminar at IIT Kanpur, 2011.
7. Murray Lecture, Society for Experimental Mechanics, 2011.
8. Seminar at University of Southern California, 2012.

APPENDIX-1

Collaborated with Professor Miladin Radovic, Texas A&M University (MURI), on the High Strain-rate Deformation Behavior of Nanolaminated Titanium Aluminum Carbide.

Effect of Strain-rate and Temperature on Dynamic Deformation of Nanolaminated Ti_2AlC

Sandeep Abotula[1], Sandip Basu[2], Miladin Radovic[2,3,*] and Arun Shukla[1]

[1]*Department of Mechanical, Industrial and Systems Engineering, University of Rhode Island, Kingston, RI 02881, USA*
[2] *Materials Science and Engineering Program, Texas A&M University, College Station, TX 77843, USA*
[3] *Department of Mechanical Engineering, Texas A&M University, College Station, TX77843, USA*

** Corresponding Author: mradovic@tamu.edu*

Abstract

Nanolaminated ternary carbide, Ti_2AlC, was characterized under dynamic loading using Split Hopkinson Pressure Bar (SHPB) compression apparatus. The dynamic loading experiments were performed in the strain-rate range of 1500-4200s^{-1} and at temperatures ranging from room temperature (RT) to 1150°C. At room temperature, the failure stress and strain show little dependence on strain rate, whereas the failure stress drops considerably at temperatures above 900°C. At all strain rates and temperatures, Ti_2AlC exhibits softening after failure initiation and a more graceful failure due to delamination and kink band (KB) formation. At temperatures higher than 900°C, grain boundary decohesion is suggested to contribute towards the decrease in the failure stress.

Introduction

Nanolaminated ternary carbides and nitrides, known as MAX phases, have attracted recent attention because of their potential for application in extreme environments. They have a general formula of $M_{n+1}AX_n$ (n = 1, 2, 3), where M is an early transition metal, A is a group-A element and X is either C or N [1-3]. Titanium aluminum carbide, Ti_2AlC, one of the well characterized compounds with M_2AX chemistry, is lightweight (4.11 g/cm^3) material with high Young's modulus (278 GPa), excellent electrical and thermal conductivity, high oxidation and corrosion resistance [1, 4-9]. Like most MAX phases, Ti_2AlC is relatively soft (Vickers hardness of ~ 4 GPa) [10] and easily machinable [11] compared to binary transition metal carbides. Because of their nanolaminated structure and kinking mechanism, Ti_2AlC is also exceedingly damage tolerant and thermal shock resistant, [12] and most likely creep, [13-15] and fatigue-resistant [16-18] like some other MAX phases.

One of the interesting aspects of MAX phases in general, and Ti_2AlC in particular is unusual deformation behavior that can be traced back to their nanolaminated hexagonal crystal structure with high c/a ratio and presence of the relatively large number of movable dislocations. The dislocations, being confined to only parallel basal planes, give rise to extensive kinking and delamination in MAX phases upon deformation [15, 19]. At room temperature, Ti_2AlC, similar to other MAX phases, shows nonlinear stress-strain behavior with fully reversible hysteresis loops and significant amount of energy dissipation under quasi-static cycling loading-unloading [15, 20-23]. Recently, a microscale model, based on nucleation, growth and annihilation of reversible nest of movable dislocations, so called incipient kink bands (IKBs), has been proposed to explain the stress-strain hysteresis in MAX phases [15, 24-25]. At higher stresses or higher temperature, the IKBs transform into permanent kink bands (KBs). Formation of KB along with delamination has been argued in literature to be the primary reason for excellent damage tolerance of MAX phases [16-17, 19]. At higher temperatures, i.e. above 1000°C, Ti_2AlC, undergoes a brittle-to-plastic (BTP) transition and strains as large as 12% can be reached before failure during compressive loading [26]. Although significant progress has been made in the recent years on understanding mechanical behavior of Ti_2AlC and other MAX phases under quasi-static conditions, we are unaware of any studies published in the open literature on the effect of high strain rate deformation behavior of Ti_2AlC at room or elevated temperatures.

In this paper we demonstrate that Ti_2AlC exhibits strain rate independent deformation behavior below BTP transition temperature up to very high strain rates under dynamic conditions. The maximum stress in the dynamic true stress-strain curves, corresponding to the failure initialization, is comparable with that measured in quasi-static experiments. Above BTP transition temperature, maximum stress measured in dynamic conditions was found to decrease significantly, in the similar way as in quasi–static testing.

Material and Specimen Geometry

Dense Ti_2AlC, with a grain size of ~100 μm, was processed by hot pressing Ti_2AlC powders (3-ONE-2, Voorhees, NJ) in graphite die at 1500°C and 20 MPa for 4 hour in the vacuum of 10^{-2} torr. Dynamic compression experiments were carried out on cylindrical specimens having 10.16 mm in diameter and 5.33 mm thick for room temperature (RT) measurements, and 6.35 mm in diameter and 3.175 mm thick for measurements at elevated temperatures.

Experimental Details

Dynamic Characterization

A Split Hopkinson Pressure Bar (SHPB) apparatus as shown in Fig. 1 with incident and transmission bars, made of Maraging steel, having a diameter and length of 12.7 mm

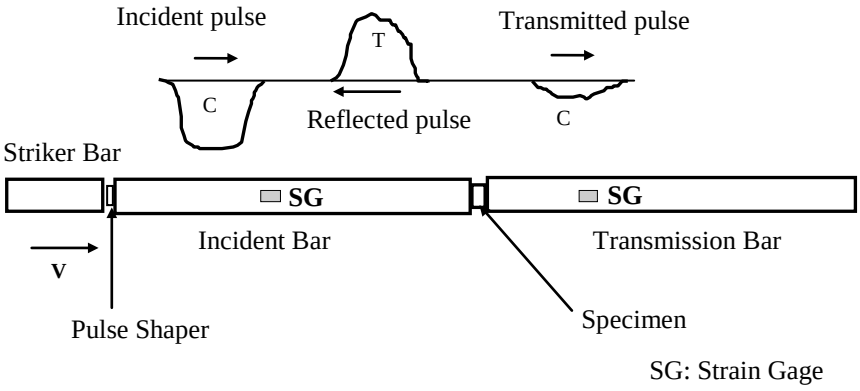

Fig. 1 Experimental setup of SPHB

and 1220 mm, respectively, was used to study the dynamic behavior of Ti_2AlC. A clay pulse shaper of thickness of 2 mm was placed at the impact end of the incident bar to improve force equilibrium conditions at the specimen-bar interface. The theoretical and experimental details of SHPB are given elsewhere [27-29]. By varying the velocities of the striker bar, room temperature experiments were carried out at strain rates ranging from 1500-4200s^{-1}. Using one-dimensional wave theory, the engineering stress and strain in the specimen can be determined from the transmitted and reflected strain pulses respectively as given in Eqs. 1 and 2.

$$\sigma_s = E_b \frac{A_b}{A_s} \varepsilon_t(t) \tag{1}$$

$$\varepsilon_s = \frac{-2c_b}{L_s} \int_0^t \varepsilon_r(t)dt \tag{2}$$

where, ε_r and ε_t represent reflected and transmitted strains respectively, c_b, E_b and A_b represent wave speed, Young's modulus and cross sectional area of the bar respectively, σ_s, ε_s, A_s, and L_s represent stress, strain , cross sectional area and length of the specimen respectively, and t represents the time. Equations (1) and (2) were suitably modified to obtain the true stress and true strain in the material.

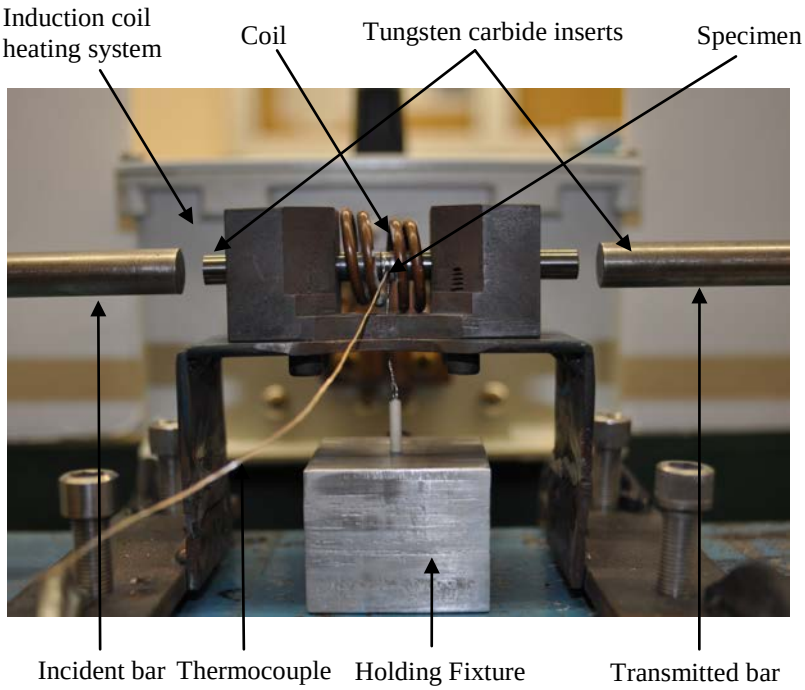

Fig. 2 Experimental setup of SHPB apparatus with induction coil heating system and holding fixture

For experiments at elevated temperatures, the SHPB apparatus in conjunction with the induction coil heating system as shown in Fig. 2 was utilized. A special fixture was designed and fabricated to load the specimen. Two tungsten carbide inserts were placed between the two pressure bars and the specimen was sandwiched between the tungsten carbide inserts as shown in Fig. 2. The inserts were used to eliminate the temperature gradient in the bars and thus protect the strain gages mounted on them. The impedance of the inserts was matched with the bars; hence they do not disturb the stress wave profiles in the bar. The impedance matching requires the diameter of these tungsten carbide inserts to be smaller than the main pressure bars. This is the reason for the specimen diameter for high temperature testing being smaller than that for room temperature testing. The bars were kept apart initially, later the specimen and carbide inserts were heated in isolation to the desired temperature (usually about 20-50°C higher than the test temperature) and soon after the bars were brought manually into contact with the specimen. The temperature of the specimen was monitored using a 0.127mm chromel-alumel thermocouple, which was spot welded onto the specimen. In most of the

experiments, it takes less than two minutes to heat the specimen to the required temperature and it takes less than 10 seconds to bring the pressure bars into contact with the tungsten inserts and fire the gun [28, 29]. High temperature experiments were carried out from RT to 1150°C under identical strain rate of about $3500s^{-1}$.

Experimental Results

Dynamic Constitutive Response at Room Temperature

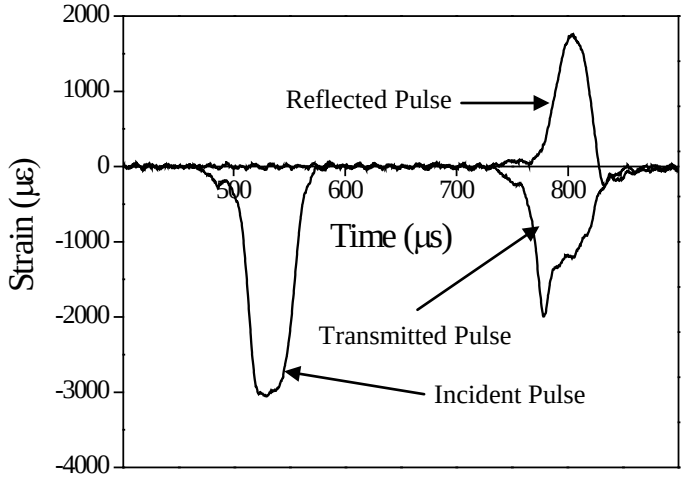

Fig. 3 Typical real-time strain pulses obtained from strain gages mounted on the bars for an average strain rate of $2800s^{-1}$

The real time strain-pulses obtained for Ti_2AlC at an average strain rate of $2500s^{-1}$ are shown in Fig 3. The clay pulse shaper used in all these experiments helped to reduce high frequency oscillations in the incident stress wave and improved the force equilibrium conditions at the specimen-bar interface.

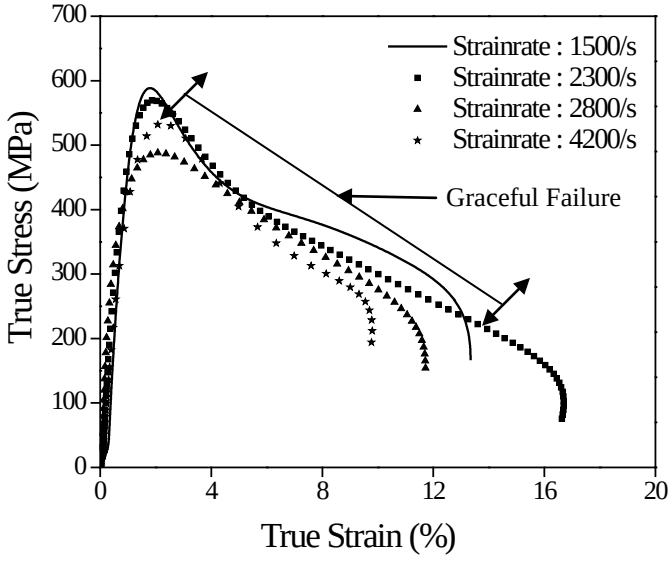

Fig. 4(a)

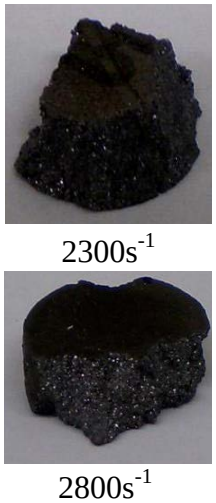

Fig. 4(b)

Fig. 4(a) True compressive stress-strain curve of Ti_2AlC under dynamic loading at room temperature. **Fig. 4(b)** show the samples tested at strain rates of $2300s^{-1}$ and $2800s^{-1}$.

The dynamic true stress-true strain curves for Ti_2AlC at room temperature for different strain rates ranging from $1500s^{-1}$ to $4200s^{-1}$ are plotted in Fig 4(a). For all strain rates, the maximum dynamic compressive stress of 480 – 600 MPa is attained around 2% true strain, followed by a stress relaxation up to maximum true strain of 9-16%. Unlike most ceramics, and similar to quasi-static experiments [30], Ti_2AlC exhibits a more graceful failure rather than brittle failure under dynamic loading (Fig. 4(b)). More interestingly, the maximum stress during the deformation of Ti_2AlC does not depend significantly on the strain rate during dynamic experiments. The slight variation observed in the maximum stress may be due to the difference in pre-existing defect concentration in the samples. The adiabatic nature of dynamic tests may also affect dislocation nucleation and propagation, which in turn can result in decrease in maximum stress with increase in strain rates. There is some evidence that the energy absorbed by the material decreases marginally with increasing strain-rates. This is indicated by the decrease in area under stress-strain curve. However, the material still exhibits graceful failure. These comments notwithstanding, more work is needed to understand the small variations in true stress-true strain curves with increasing strain rates. Fig. 5 shows the real-time deformations of Ti_2AlC under dynamic loading at room temperature for a strain rate of $2800s^{-1}$. At t=50 μs, the crack initiates at the lower right of the specimen, and starts propagating through the specimen as shown in Fig 5. By t=100 μs, more cracks are clearly visible and they have completely propagated through the specimen. After this time, the damage begins to grow and the outer edge of the specimen breaks off, while the center part of the specimen stays intact.

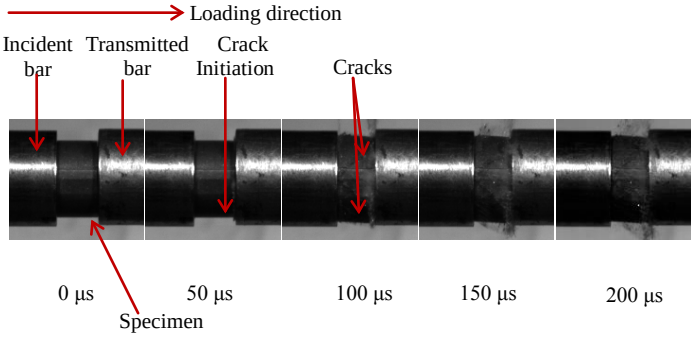

Fig. 5 Real time deformations of Ti_2AlC under dynamic loading for a strain rate of $2800s^{-1}$

Scanning Electron Microscopy, SEM, images of the fracture surfaces in Figures 6(a) and 6(b) show extensive delamination and KB formation along the fracture surface after testing of Ti_2AlC at strain rates of $2300s^{-1}$ and $2800s^{-1}$, respectively. The high density of KBs found in the fracture surfaces imply significant amount of plastic deformation during crack propagation, which in turn is evident from the graceful failure shown in Fig. 4(a). As the strain-rate increases, the intensity of KB formation decreases slightly and resulting in the decrease of the dissipation energy. It is interesting to note here that, similar to quasi-static deformation, no evidence of KB has been observed in the polished cross-sections of the interior of the samples (not shown here). This suggests that

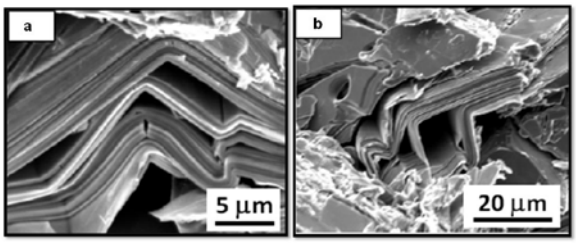

Fig. 6(a) $2300s^{-1}$ Fig. 6(b) $2800s^{-1}$

Fig. 6 Results of SEM images showing extensive kink band formation and delamination for the samples tested at strain-rates of (a) $2300s^{-1}$ and (b) $2800s^{-1}$.

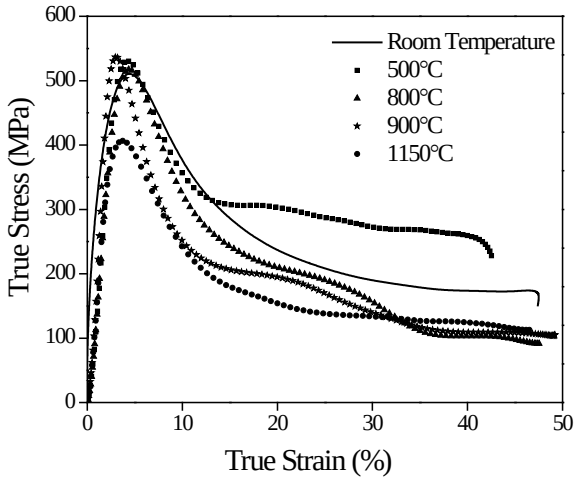

Fig. 7(a)

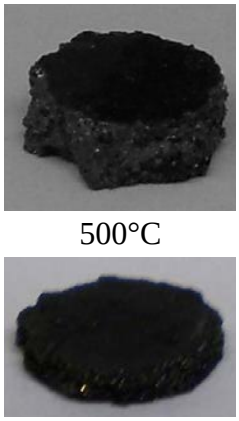

Fig. 7(b)

Fig. 7(a) True compressive stress-strain curve of Ti_2AlC under dynamic loading at elevated temperatures and a strain rate of about $3500s^{-1}$

if incipient kink bands (IKBs) which are reversible in nature form inside the favorably oriented grains during high strain rate deformation, they do not develop in full KB and disappear upon unloading. However, these IKBs transform to fully developed KBs along the fracture surfaces. Since formation of KBs (Figures 6(a) and 6(b)) and delamination dissipate significant amount of energy, it hinders the crack propagation and results in graceful failure of Ti_2AlC even at strain rates as high as $4200s^{-1}$.

The dynamic true stress-strain curves for Ti_2AlC tested at a strain rate of $3500s^{-1}$ and different temperatures are shown in Figure 7(a) Initially, as the temperature increases from room temperature to 900°C, there is no significant change in the maximum compressive strength (about 520-540 MPa). However, at 1150°C, the material shows a significant decrease in the maximum true compressive strength to around 400 MPa. For all the temperatures, the failure initiates at a true strain of ~4% and reaches a maximum true strain of 45-50%. Since the diameter of the specimen for high temperature testing is smaller in comparison to the room temperature testing the resulting stress on the sample for a given loading is higher and this results in larger strains [29]. Even at high temperatures, the material exhibits graceful failure (Fig. 7(b)). Fig. 8 shows the real-time deformations of Ti_2AlC under dynamic loading at 500°C. Similar to room temperature experiments, the failure initiates at the peak stress and the outer edge of the specimen breaks off while the center part of the specimen remains primarily

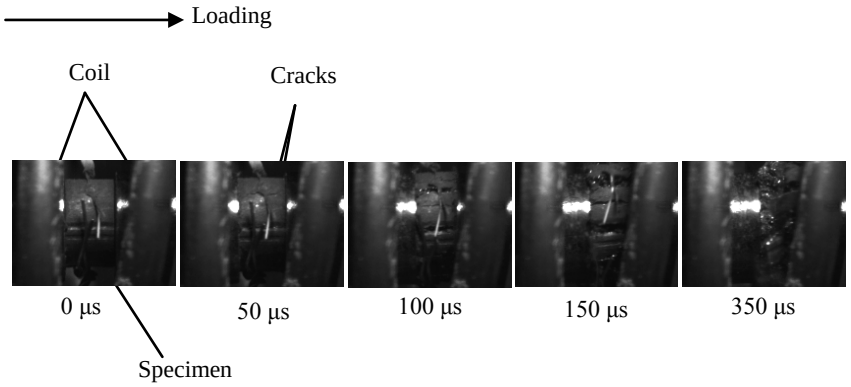

Fig. 8 Real time deformations of Ti_2AlC under dynamic loading at 500°C

intact as shown in Fig. 8. Here again, SEM micrographs from the fracture surfaces after dynamic deformation at elevated temperatures, as illustrated in Figures 9(a) and 9(b) for samples tested at 500°C and 1150°C respectively, reveal large amount of kinking. It is important to note here that it is difficult to infer from the fracture surfaces whether the amount of plastic deformation by kinking depends on the testing temperature. However, the drop in maximum stress clearly indicates that the material softens, i.e. undergoes brittle-to-plastic transition at temperatures above 900°C even at deformation rates of $3500s^{-1}$.

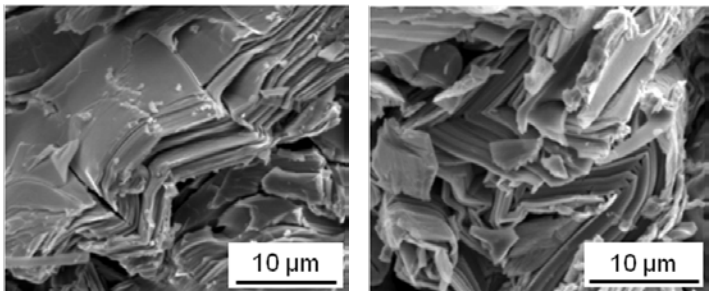

Fig. 9(a) 500°C Fig. 9(b) 1150°C

Fig. 9 Results of SEM images showing extensive kink band formation and delamination for the samples tested at strain-rates of (a) 500°C and (b) 1150°C.

The later is even more obvious when the change in maximum stress with temperature for the dynamic experiments is plotted, Figure 10. For comparison, the change in maximum stress from quasi-static tests [10] at $10^{-4}s^{-1}$ is also plotted in the same graph. The similar nature of change in maximum stress for both strain rates again confirms our conclusion that deformation in Ti_2AlC is quite strain-rate insensitive below BTP transition temperature even when strain rates are as high as $3500s^{-1}$. More importantly, Figure 10 suggests that the material goes through the same BTP transition at strain rates that are orders of magnitude different from each other.

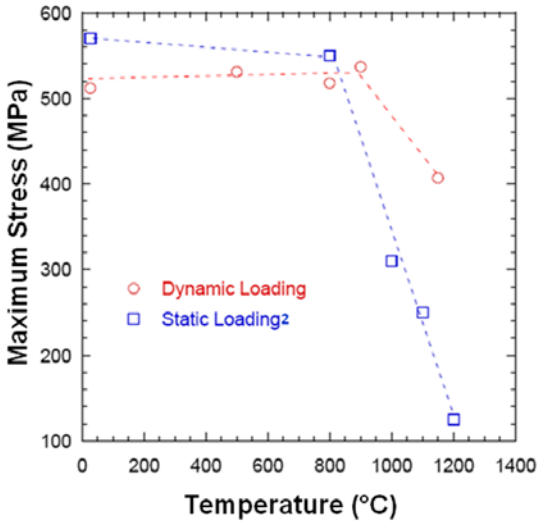

Fig. 10. Effect of temperature on the maximum stress during the dynamic deformation of Ti_2AlC. The quasi-static compressive strengths at different temperatures, from Ref. 10, are also plotted for comparison.

As far as we are aware this is the first report on dynamic stress-strain behavior of Ti_2AlC at different strain rates and temperatures, and thus more work is needed to fully understand observed trends. However, taking into account structural and mechanical similarities between the Ti_2AlC and Ti_3SiC_2, for which effect of strain rate (of the order of $10^{-7} – 10^{-4}s^{-1}$) has been extensively studied [31], it is not unreasonable to assume that both of them would behave in a qualitatively similar way. Below the BTP transition temperature, Ti_3SiC_2 exhibits brittle deformation with fully reversible hysteresis at low strains, and maximum stresses that are almost independent on the deformation rate. The hysteretic behavior is shown to be due to reversible motion of dislocations in parallel slip planes, and has been discussed in more details elsewhere [15,

20]. Above the BTP transition temperature, the deformation in Ti_3SiC_2 depends on the strain rate. For example, maximum stress in Ti_3SiC_2 shows strain rate dependency in the 1100 – 1200^oC temperature range for strain rates below $10^{-6}s^{-1}$. However, above a strain rate of 10^{-5}/s, there is little effect of strain rate on maximum stress, and Ti_3SiC_2 behaves as a brittle solid. Hence, like in quasi-static experiments, the primary reason for decrease in stress above BTP can be argued to be grain boundary decohesion and/or extensive delamination. Thus, further work on understanding the role of grain boundaries on the dynamic stress-strain behavior of MAX phases in general and Ti_2AlC in particular, will shed more light on the nature of maximum stress decrease above BTP transition temperature.

Conclusions

In conclusion, stress-strain analysis along with microscopic investigation of the fracture surfaces in nanolaminated Ti_2AlC under dynamic loading reveal that, like quasi-static conditions, the underlying failure mechanism is independent of strain rate at temperatures below 900^oC and that it is predominantly controlled by delamination of the nanolaminated structure and KB formation. At temperatures higher than 900^oC, grain boundary decohesion plays an important role in crack propagation, and subsequently in decrease of failure stress.

Acknowledgements

This work was supported in part by the Air Force Office of Scientific Research under the MURI Award No. FA9550-09-1-0686 at the Texas A&M University, and by the Grant No. FA9550-09-1-0639 at the University of Rhode Island.

References

[1] M. W. Barsoum, Prog. Solid State Chem **28,** 201 (2000).
[2] J. Wang and Y. Zhou, Annual Review of Materials Research **39,** 415 (2009).
[3] P. Eklund, M. Beckers, U. Jansson, H. Högberg, and L. Hultman, Thin Solid Films **518,** 1851 (2010).
[4] J. D. Hettinger, S. E. Lofland, P. Finkel, T. Meehan, J. Palma, K. Harrell, S. Gupta, A. Ganguly, T. El-Raghy, and M. W. Barsoum, Phys. Rev. B **72,** 115120 (2005).
[5] M. W. Barsoum, J. Electrochem. Soc. **148,** C544 (2001).
[6] M. W. Barsoum, N. Tzenov, A. Procopio, T. El-Raghy, and M. Ali, J.. Electrochem. Soc., **148,** C551 (2001).
[7] X. H. Wang and Y. C. Zhou, Oxidation of Metals **59,** 303 (2003).
[8] M. Sonestedt, J. Frodelius, M. Sundberg, L. Hultman, and K. Stiller, Corrosion Science **52,** 3955 (2010).
[9] J. Byeon, J. Liu, M. Hopkins, W. Fischer, N. Garimella, K. Park, M. Brady, M. Radovic, T. El-Raghy, and Y. Sohn, Oxidation of Metals **68,** 97 (2007).
[10] F. L. Meng, Y. C. Zhou, and J. Y. Wang, Scripta Materialia **53,** 1369 (2005).
[11] M. W. Barsoum, D. Brodkin, and T. El-Raghy, Scrip. Met. et. Mater. **36,** 535 (1997).
[12] T. El-Raghy, A. Zavaliangos, M. W. Barsoum, and S. R. Kalidindi, J. Amer. Cer. Soc. **80,** 513 (1997).

[13] M. Radovic, M. W. Barsoum, T. El-Raghy, and S. M. Wiederhorn, Acta Mater. **49,** 4103 (2001).
[14] M. Radovic, M. W. Barsoum, T. El-Raghy, and S. M. Wiederhorn, J. Alloys and Compds. **361,** 299 (2003).
[15] M. W. Barsoum and M. Radovic, Annual Review of Materials Research **41,** 195 (2011).
[16] C. J. Gilbert, D. R. Bloyer, M. W. Barsoum, T. El-Raghy, A. P. Tomasia, and R. O. Ritchie, Scripa Materialia **238,** 761 (2000).
[17] D. Chen, K. Shirato, M. W. Barsoum, T. El-Raghy, and R. O. Ritchie, J. Amer. Cer. Soc. **84,** 2914 (2001).
[18] H. Zhang, Z. G. Wang, Q. S. Zang, Z. F. Zhang, and Z. M. Sun, Scripta Mater. **49,** 87 (2003).
[19] M. W. Barsoum, L. Farber, T. El-Raghy, and I. Levin, Met. Mater. Trans. **30A,** 1727 (1999).
[20] M. W. Barsoum, T. Zhen, S. R. Kalidindi, M. Radovic, and A. Murugahiah, Nature Materials **2,** 107 (2003).
[21] A. G. Zhou, M. W. Barsoum, S. Basu, S. R. Kalidindi, and T. El-Raghy, Acta Mater. **54,** 1631 (2006).
[22] A. G. Zhou and M. W. Barsoum, Journal of Alloys and Compounds **498,** 62 (2010).
[23] M. W. Barsoum, T. Zhen, A. Zhou, S. Basu, and S. R. Kalidindi, Phys. Rev. B. **71,** 134101 (2005).
[24] M. W. Barsoum and S. Basu, in *Encyclopedia of Materials: Science and Technology*, edited by K. H. J. Buschow, R. W. Cahn, M. C. Flemings, B. Ilschner, E. J. Kramer, S. Mahajan, and P. Veyssiere (Elsevier, 2010).
[25] A. G. Zhou, S. Basu, G. Friedman, P. Finkel, O. Yeheskel, and M. W. Barsoum, Physical Review B **82,** 094105 (2010).
[26] Y. C. Zhou and X. H. Wang, Materials Research Innovations **5,** 87 (2001).
[27] H. Kolsky, Proceedings of the Physical Society. Section B **62,** 676 (1949).
[28] A. Kidane and A. Shukla, Journal of Materials Science **43,** 2771 (2008).
[29] S. Abotula, A. Shukla, and R. Chona, Journal of Materials Science **46,** 4971 (2011).
[30] M. W. Barsoum, M. Ali, and T. El-Raghy, Met Mater Trans **31A,** 1857 (2000).
[31] M. Radovic, M. W. Barsoum, T. El-Raghy, S. M. Wiederhorn, and W. E. Luecke, Acta Materialia **50,** 1297 (2002).

APPENDIX-2

Collaboration with Professor William G. Fahrenholtz, Missouri University of Science and Technology, on the High Strain-rate Deformation behavior of ZrB_2

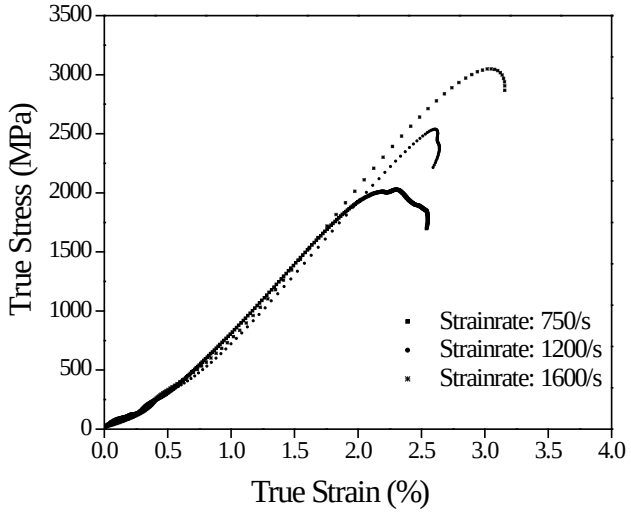

Fig. 11 True compressive stress-strain curve of ZrB_2-SiC under dynamic loading at room temperature

A series of experiments were conducted to study the dynamic compressive behavior of ZrB_2-SiC at different strain rates. Split Hopkinson pressure bar apparatus as shown in Figure 1 (Appendix-1) was used for applying dynamic loads. Experiments were performed for three different strain rates ranging from 750-1600s^{-1}. Initial results are shown in Fig. 11. None of the specimens failed under applied stress at these strain rates.